IOP Publishing Smart Materials and Structures
Smart Mater. Struct. 24 (2015) 105032 (10pp) doi:10.1088/0964-1726/24/10/105032

On the use of tensegrity structures for kinetic solar facades of smart buildings

F Fraternali[1,3], E De Chiara[1] and R E Skelton[2]

[1] Department of Civil Engineering, University of Salerno, I-84084 Fisciano (SA), Italy
[2] Department of Mechanical and Aerospace Engineering, University of California at San Diego, La Jolla, CA 92093-0411, USA

E-mail: f.fraternali@unisa.it, elenadechiara@gmail.com and bobskelton@ucsd.edu

Received 22 May 2015, revised 10 August 2015
Accepted for publication 14 August 2015
Published 18 September 2015

Abstract

We investigate the use of tensegrity structures with morphing and prestress-stability capabilities for the design of active solar façades of smart buildings. Morphing tensegrity lattices are used to design shading screens composed of umbrella-shaped 'eyes' that are opened and closed by adjusting the elongation in a limited number of cables. Prestressable lattices are instead employed to design superstable Venetian blinds that are composed of orientable slats. Future use of tensegrity solutions for next-generation smart buildings are outlined, with the aim of designing kinetic solar façades that combine morphing abilities with prestress-stability.

S Online supplementary data available from stacks.iop.org/SMS/24/105032/mmedia

Keywords: tensegrity, solar facades, morphing structures

(Some figures may appear in colour only in the online journal)

1. Introduction

It is known that the construction industry significantly contributes to overall energy consumption (up to 40% in the European Union, see [1], and directive 31/2010/UE) and there is an urgent need for sustainable buildings that are able to reduce CO_2 emissions by 90% and energy consumption by as much as 50% [2]. Renewable energy technologies have significant deployment potential as resources are spread globally, in contrast to the conventional sources such as gas, coal and oil, which are more geographically concentrated. Renewable generation is estimated to rise to 25% of gross power generation in 2018, up from 20% in 2011 as deployment spreads out globally [1].

The demand for energy efficient buildings calls for the adoption of active façades that are able to mitigate air conditioning consumption resulting from direct exposure to solar rays, and to harvest wind and solar energy through on-site wind power generators [3], building integrated photovoltaic (BIPV) systems, and/or solar hot water panels [4–7]. The so-called solar-architecture nowadays explores the use of flexible envelopes governed by smart control systems to adjust heating, ventilation, thermal isolation, lighting and shading of energy efficient buildings according to weather conditions and seasons (see e.g., [7] and references therein). The building of the future also needs to be safer with respect to natural hazards, such as earthquakes and high winds, and more energy efficient in terms of making components and subsystems multidisciplinary (e.g., combining structural design with heating, ventilation and air conditioning design) [8, 9].

Two main categories of solar façades are recognized in the literature: opaque and transparent–translucent façades, and both types can be either active or passive [5, 6]. Opaque façades actively or passively absorb and reflect sun rays [5], while transparent and translucent façades are able to combine absorption and reflection (translucent façades) mechanisms with direct transfer of solar heat gain into the building [6]. Active opaque façades include BIPV, solar-thermal (BIST), and photovoltaic/thermal (BIPV/T) systems; while passive opaque façades consist of either thermal storage walls or solar chimneys [5]. Active opaque façades make use of electrical and/or mechanical devices to transfer the gained solar energy

[3] Author to whom any correspondence should be addressed.

into the building (in the form of thermal or electrical energy), while passive opaque façades directly transform the incident sunlight into thermal energy. Active transparent and translucent façades comprise mechanically ventilated transparent façades, and semi-transparent BIPV, BIST and BIPV/T systems, while passive transparent and translucent systems essentially consist of naturally ventilated façades.

Receiving increased attention are active solar systems consisting of double (or multiple) glazed façades that incorporate Venetian blinds (also known as double skin façades or DSFs) [6, 10–14]. Such systems overcome the advantages of single (fully) glazed facades due to high energy consumption and excessive noise permeability [10]. The use of natural or forced ventilation into the cavity between the external and internal glazing; the optimal design of the position of the blinds [11]; sun-tracking abilities of the blind slats; and the adoption of photovoltaic module integrated blinds (PV-blinds) [12], may significantly reduce heating and cooling energy needs of buildings equipped with DSFs [10, 13]. It is worth noting that the use of forced ventilation within the cavity of DSFs may require the adoption of wind-stable Venetian blinds [14], which are also needed in the case of external blinds [15–17]. Commercially available solutions for wind-stable Venetian blinds are usually equipped with slats moving on special profile rails [17]. Such systems are affected by significantly large friction effects, due to the multiple contacts between the slats and the rails, and interlocking effects between the slats [17].

Innovative shading screens have been recently designed by Aedas Architects for the Al Bahar Towers in Abu Dhabi [18]. These screens consist of curtain walls placed two meters outside the towers' façades, and are intended to mimic the shading lattice-work 'mashrabiya'. The mashrabiya screens are composed of more than one thousand 'origami' eyes in fiberglass, which are opened (i.e., folded out) at night, and are progressively closed during daylight hours, through a piston-actuated, computer-controlled technology. The screens are designed to reduce the solar irradiation of the towers by more than 50%, and to produce marked decreases in air conditioning consumption, since Abu Dhabi temperatures can increase up to 50 degrees Celsius in summer.

The present work investigates the use of tensegrity structures to form active solar façades of next generation smart buildings. Tensegrity systems are prestressable truss structures, which are obtained by connecting a network of compressive members (bars or struts) through a set of stabilizing cables (or strings) under tension [9]. Tensegrity architectures appear in a variety of natural shapes [9], and have been employed for different engineering uses [19–22]. It has been recognized that tensegrity systems are lightweight, easy to control and to deploy, and that the adoption of tensegrity concepts may lead to the design of minimal mass structures under different loading conditions [9, 23]. There is also the question of their easy integration into solar and acoustical panels, which can be physically identified with special rigid members of the structure.

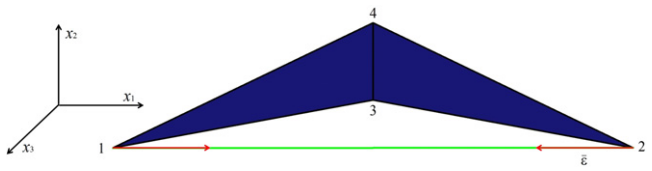

Figure 1. Elementary truss lattice.

We begin in section 2 by studying the actuation mechanisms of tensegrity lattices, with special focus on morphing and superstable lattices. Next, we investigate the use of morphing and superstable lattices as components of kinetic facades of smart buildings. We first design a tensegrity solution for the active shading screens similar to those used in Al Bahar Towers in Abu Dhabi (section 3). We continue in section 4 with the design a superstable tensegrity structure, which mimics a Venetian blind, and provides support for wind-stable slats. Future perspective of the present study are drawn in section 5, while concluding remarks are presented in section 6.

2. Actuation of tensegrity lattices

2.1. Morphing lattices

Let us examine the motion of the elementary truss lattice shown in figure 1. The elongation rate of the mth element connecting nodes i and j is given by:

$$\dot{e}_m = \left(\dot{\boldsymbol{u}}_j - \dot{\boldsymbol{u}}_i\right) \cdot \boldsymbol{a}_m, \tag{1}$$

where $\boldsymbol{a}_m$ is the unit vector parallel to the element at the current time t (pointing towards node j); $\dot{\boldsymbol{u}}_i$ and $\dot{\boldsymbol{u}}_j$ are the velocity vectors of the nodes i and j, respectively; and ℓ_m is the length of the element at time t. We assume that the lattice has N nodes and M members.

On introducing an arbitrary Cartesian frame, we let $\bar{\mathrm{x}}_{i_n}$ denote the Cartesian components of node i in correspondence with the unstressed (or natural) configuration of the lattice, and let u_{i_n} denote the Cartesian components of the displacement vector of the same node ($n = 1, 2, 3$). Making use of the dot notation for time derivatives, we collect the Cartesian components of the velocity vectors of the different nodes into the following array with $3N$ entries

$$\dot{\boldsymbol{u}} = \left[\dot{u}_{1_1}\, \dot{u}_{1_2}\, \dot{u}_{1_3} \ldots\ \dot{u}_{N_1} \dot{u}_{N_2} \dot{u}_{N_3}\right]^{\mathsf{T}}, \tag{2}$$

T denoting the transposition symbol. Similarly, we collect the elongation rates of all lattice members into the following array with M entries

$$\dot{\boldsymbol{e}} = \left[\dot{e}_1 \ldots\ \dot{e}_M\right]^{\mathsf{T}}. \tag{3}$$

It is an easy task to write the compatibility equations (1) in matrix form, obtaining

$$C\,\dot{\boldsymbol{u}} = \dot{\boldsymbol{e}}, \tag{4}$$

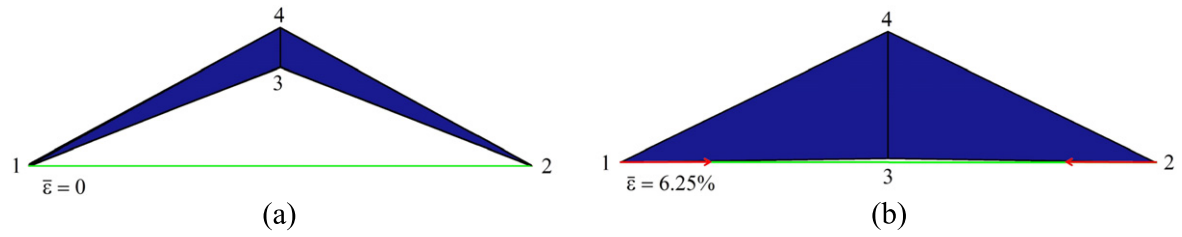

Figure 2. Motion produced by the actuation of the string 1-2: (a) string 1-2 unstretched; (b) string 1-2 stretched to 6.25%.

where $\boldsymbol{C}$ denotes the $M \times 3N$ compatibility matrix with current entry equal to $\partial \ell_m / \partial u_{i_n}$, and ℓ_m is computed as follows

$$\ell_m = \sqrt{\sum_{n=1}^{3} \left[\left(\bar{x}_{j_n} + u_{j_n} \right) - \left(\bar{x}_{i_n} + u_{i_n} \right) \right]^2}. \tag{5}$$

We now assume that a given number P of velocity components are forced to be zero, due to the presence of externals constrains limiting the possibilities of motion of the lattice. By suitably sorting the velocity vector $\dot{\boldsymbol{u}}$, we can rewrite the matrix equation (4) as

$$\left[\boldsymbol{C}_1 \ \vdots \ \boldsymbol{C}_2 \right] \begin{bmatrix} \dot{\boldsymbol{u}}_1 \\ \cdots \\ \dot{\boldsymbol{u}}_2 \end{bmatrix} = \dot{\boldsymbol{e}}, \tag{6}$$

where $\dot{\boldsymbol{u}}_1$ is the array with $Q = (3N\text{-}P)$ entries that collects the unconstrained velocity components; $\dot{\boldsymbol{u}}_2$ is the P-dimensional array collecting the nodal velocity components constrained to zero; $\boldsymbol{C}_1$ is a $M \times$ Q submatrix of $\boldsymbol{C}$; and $\boldsymbol{C}_2$ is the complementary $M \times$ P submatrix of $\boldsymbol{C}$. In minimal coordinates, the compatibility equations of the constrained lattice are then written as

$$\mathbf{B}\, \dot{\boldsymbol{q}} = \dot{\boldsymbol{e}} \tag{7}$$

with $\mathbf{B} = \boldsymbol{C}_1$ (instantaneous *kinematic matrix* of the lattice [24]), and $\dot{\boldsymbol{q}} = \dot{\boldsymbol{u}}_1$.

We say that the lattice is *morphing* [25], if it follows

$$r = M = Q \tag{8}$$

r denoting the rank of the kinematic matrix $\mathbf{B}$. Under the assumption (8), the system of compatibility equation (6) has unique solution $\dot{\boldsymbol{q}} \in \mathbb{R}^{\boldsymbol{Q}}$ for any given $\dot{\boldsymbol{e}} \in \mathbb{R}^{\boldsymbol{M}}$, $\mathbb{R}$ denoting the set of real numbers. As a consequence, in a morphing lattice, one can produce the motion of the structure by actuating a single element, i.e., by prescribing that a single entry of $\dot{\boldsymbol{e}}$ is nonzero. Such a result implies the actuation of morphing lattices requires minimal storage of internal energy [25]. Given an 'actuation' history $\dot{\boldsymbol{e}} = \dot{\tilde{\boldsymbol{e}}}$, the positions of the vertices of a morphing lattice at the current time t are computed from the integral equation

$$\boldsymbol{q} = \int_0^t \dot{\boldsymbol{q}}\, \mathrm{d}t = = \int_0^t \mathbf{B}^{-1}\, \dot{\tilde{\boldsymbol{e}}}\, \mathrm{d}t \tag{9}$$

$\mathbf{B}^{-1}$ denoting the inverse of the kinematic matrix $\mathbf{B}$ in correspondence with the current configuration of the lattice, which exists and is unique under the assumption (**8**).

Assuming the action of quasi-stating loading and making use of the principle of virtual work, it is an easy task to obtain the following expression of the equilibrium problem of the lattice [9, 25]

$$\boldsymbol{A}\boldsymbol{t} = \boldsymbol{f}, \tag{10}$$

where $\boldsymbol{A} = \mathbf{B}^{\mathsf{T}}$ is the instantaneous *static* (or *equilibrium*) *matrix* of the lattice; $\boldsymbol{t} \in \mathbb{R}^{\boldsymbol{M}}$ is the array collecting the axial forces carried the lattice elements (or *bar tensions* [24]), and $\boldsymbol{f} \in \mathbb{R}^{\boldsymbol{Q}}$ is the array of the active nodal forces. It follows from (7) that a morphing lattice is statically and kinematically determinate (or *isostatic*) [24]. It is worth remarking that we can design structures that can change their shape (i.e., have morphing abilities, in a generalized sense) by controlling strings that are not statically determinate. The example presented in section 4 shows that, in a statically and kinematically indeterminate structure, it is possible to produce motions that preserve the rigidity of the compressed members and at the same time keep the structure stable against undesired mechanisms by the suitable pre-tensioning of the strings. The whole philosophy of tensegrity is largely based on such a self-stress concept [9] (see also section 2.3).

We now get back to the lattice structure in figure 1, assuming that nodes 1 and 2 are constrained to move along the lines 1-4 and 2-4, respectively, and that node 4 is constrained to move along the x_3-axis (refer to supplementary material for additional details). We also suppose that the nodes of such a structure have the following position vectors $\boldsymbol{n}_i$ $(i = 1, \ldots, 4)$ in correspondence with the open configuration of the lattice (figure 2)

$$\boldsymbol{n}_1 = \begin{bmatrix} 0.125 \\ 0.057 \\ 0.045 \end{bmatrix} m, \quad \boldsymbol{n}_2 = \begin{bmatrix} 3.875 \\ 0.057 \\ 0.045 \end{bmatrix} m,$$
$$\boldsymbol{n}_3 = \begin{bmatrix} 2.000 \\ 0.738 \\ -0.262 \end{bmatrix} m, \quad \boldsymbol{n}_4 = \begin{bmatrix} 2.000 \\ 1.000 \\ 0.968 \end{bmatrix} m. \tag{11}$$

Under such assumptions, it is not difficult to show that the structure in figure 1 is morphing and can be controlled by actuating only the string 1-2, that is, prescribing nonzero elongation rate in such an element, and zero elongation rates in all the remaining elements. This actuation mechanism leaves unchanged the lengths of the edges of the triangles 1-3-4 and 2-3-4, which therefore move rigidly over time (figure 2).

2.2. Tangent stiffness matrix and stability

A lattice is said to admit *mechanisms* at the current time t, if there exist sets of nodal velocities $\dot{\boldsymbol{q}}_M$ at that time that do not produce elongation rates in any lattice member ($\dot{\boldsymbol{e}} = 0$). Such a definition trivially implies that the kinematic matrix of the lattice $\mathbf{B}$ has nonempty null space, i.e. it results in

$$r < Q. \tag{12}$$

Concerning the constitutive response of the lattice members, we hereafter restrict our attention to truss lattices whose members can be described as linear elastic springs, such that the law relating the axial force carried by the generic member to the member length can be written as

$$t_m = k_m\left(\ell_m - \bar{\ell}_m\right), \quad m = 1, \ldots, M. \tag{13}$$

In equation (13), $\bar{\ell}_m$ denotes the *rest-length* (or *natural length*) of the member, i.e., its length in the unstressed configuration of the lattice. In the same equation, k_m denotes the *axial stiffness* of the member. It is worth noting that the constitutive assumption (13) is linear form the material point of view, and nonlinear from the geometrical point of view (St Venant–Kirchhoff model) [29]. When the generic member is made of a homogeneous material with Young modulus E_m; its cross-section has constant profile with area A_m; and the change in the cross-section area induced by the axial stretching of the member can be neglected, we write $k_m = E_m A_m / \bar{\ell}_m$.

We now substitute equation (13) into equation (10) and recall that the current entry of the equilibrium matrix is equal to $\partial \ell_m / \partial u_{i_n}$, obtaining the following expression of the generic equilibrium equation of the lattice

$$\sum_{m=1}^{M} k_m\left(\ell_m - \bar{\ell}_m\right)\frac{\partial \ell_m}{\partial q_r} = f_r. \tag{14}$$

By taking time derivatives of both sides of equation (14), we get to the incremental elastic problem of the lattice into the following form

$$\boldsymbol{K_T}\,\dot{\boldsymbol{q}} = \dot{\boldsymbol{f}}, \tag{15}$$

where $\boldsymbol{K_T}$ is the *tangent stiffness matrix* given by

$$\boldsymbol{K}_T = \boldsymbol{K}_M + \boldsymbol{K}_G \tag{16}$$

with

$$K_{M_{rs}} = k_m \frac{\partial \ell_m}{\partial q_r}\frac{\partial \ell_m}{\partial q_s},$$
$$K_{G_{rs}} = t_m \frac{\partial^2 \ell_m}{\partial q_r \partial q_s} \quad (r, s = 1, \ldots, Q). \tag{17}$$

In equation (17), $\boldsymbol{K}_M$ is known as the *material stiffness matrix* of the lattice, while $\boldsymbol{K}_G$ is known as the *geometric stiffness matrix*. Equation $(17)_1$ highlights that $\boldsymbol{K}_M$ depends on to the material stiffness coefficients $(k_1, k_2, \ldots, k_M)$ and the cosine directors of the member axes ($\frac{\partial \ell_m}{\partial q_r}$ for $m = 1, \ldots M$; $r = 1, \ldots, Q$). Equation $(17)_2$ instead reveals that $\boldsymbol{K}_G$ depends on the tensions acting in the current configurations of the lattice members $(t_1, t_2, \ldots, t_M)$, and the changes in the cosine directors of the member axes (i.e., the quantities $\frac{\partial^2 \ell_m}{\partial q_r \partial q_s}$, for $m = 1, \ldots M$; $r, s = 1, \ldots, Q$). It is easy to realize that $\boldsymbol{K}_G$ can be neglected when the structure is under zero member tensions, and/or the member lengths vary linearly with the nodal displacements $\boldsymbol{q}$ (e.g., in the case of infinitesimally-small deformations). Upon looking at the expression of $\boldsymbol{K}_M$ given by $(17)_1$, it is also easy to recognize that the material stiffness matrix can be written as

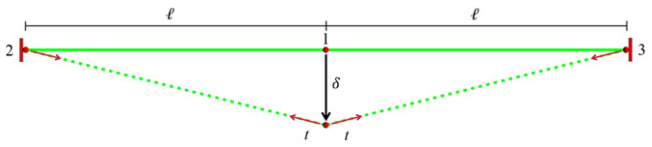

Figure 3. Elementary super-stable lattice.

$$\boldsymbol{K}_M = \boldsymbol{A}\,\mathrm{diag}\left(k_1, k_2, \ldots, k_M\right)\boldsymbol{A}^{\mathsf{T}} \tag{18}$$

which implies that its null space coincides with that of the kinematic matrix $\boldsymbol{B} = \mathbf{A}^{\mathsf{T}}$ (see also [26, 27]). Therefore, a *zero-material-stiffness mode*, defined as a virtual displacement $\boldsymbol{u}_M$ such that it results $\boldsymbol{K_M}\,\boldsymbol{u}_M = \mathbf{0}$, has the same shape as a mechanism of the lattice, coinciding with a mechanism $\dot{\boldsymbol{q}}_M$ multiplied by an infinitesimal time interval. For the sake of simplicity, hereafter we will use the term mechanism to denote both a velocity vector $\dot{\boldsymbol{q}}_M$ that lies in the null space of the kinematic matrix, and a zero-material-stiffness mode $\boldsymbol{u}_M$.

A configuration of a lattice is said to be *stable* if the tangent stiffness matrix $\boldsymbol{K_T}$ is positive-definite in correspondence with such a configuration, i.e., it results

$$\boldsymbol{K_T u} \cdot \boldsymbol{u} > 0, \tag{19}$$

where $\boldsymbol{u}$ is an arbitrary virtual displacement from the analyzed configuration (i.e., a virtual velocity $\dot{\boldsymbol{q}}$ multiplied by an infinitesimal time interval) [26–29]. A *zero-stiffness mode* is instead defined as a virtual displacement $\boldsymbol{u}$ such that the right-hand side of (19) is zero.

The lattice is said to be in a *prestress-stable* configuration, if it obeys

$$\boldsymbol{K}_G\,\boldsymbol{u}_M \cdot \boldsymbol{u}_M > 0 \tag{20}$$

in correspondence with each nontrivial mechanism ($\boldsymbol{u}_M \neq \mathbf{0}$) [26–29]. It is clear that, in such a configuration, the lattice mechanisms are not zero-stiffness modes, due to the action of stabilizing member tensions.

Finally, the lattice is said to be *superstable* if it is prestress-stable and, in addition, $\boldsymbol{K}_G$ is nonnegative in correspondence with all the virtual displacements that are not mechanisms. As a consequence of such a definition, a superstable lattice is stable along all the possible virtual displacements from the current configuration, independently of prestress and material properties [28]. The lattice in figure 1, which does not admit mechanisms (being statically determinate), is superstable and exhibits the kinematic matrix, provided as supplementary material.

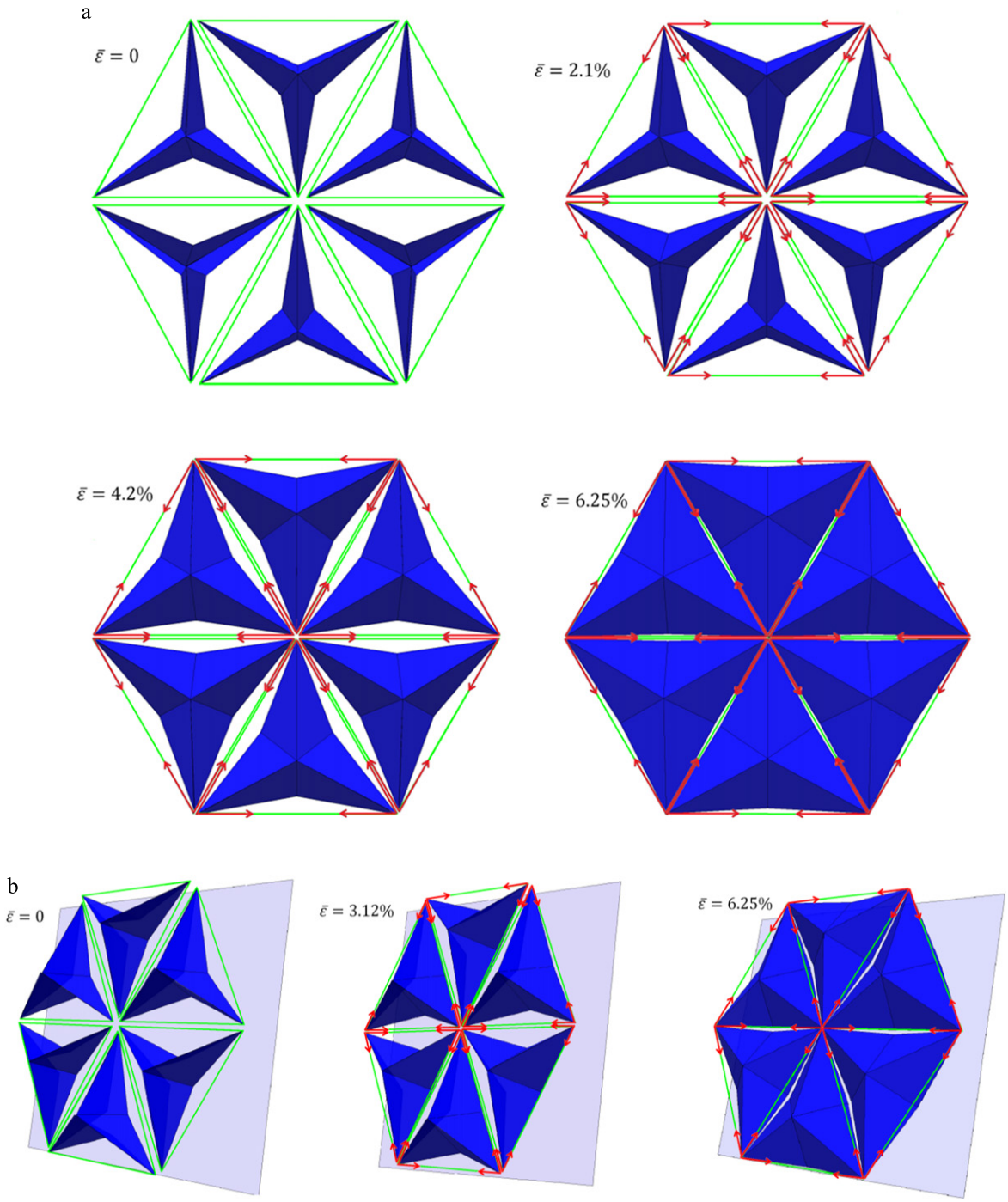

Figure 4. (a) Frontal view of the actuation mechanism of mashrabiya shading screens with tensegrity architecture available at stacks.iop.org/SMS/24/105032/mmedia. (b) 3D view of the actuation mechanism of mashrabiya shading screens with tensegrity architecture (actuation movie provided as supplementary material).

2.3. Superstable lattices with kinematic and static indeterminacies

According to condition (8), morphing lattices do not admit *states of self-stress*, i.e., nontrivial solutions $\boldsymbol{t}_s \neq \boldsymbol{0}$ of the equilibrium problem (10) under zero external forces ($\boldsymbol{f} = \boldsymbol{0}$). Lattices that instead admit such states of bar tensions are said *prestressable* [9, 26]. Trivially, the equilibrium matrix $\boldsymbol{A}$ of a prestressable lattice has nonempty null space, i.e., it obeys

$$r < M. \tag{21}$$

Let us collect the free components of an arbitrary virtual displacement of the lattice in figure 3 into the following vector with two entries $\boldsymbol{u} = [u_1, u_2]^{\mathsf{T}}$, with u_1 and u_2 respectively denoting the horizontal and vertical displacement components of node 1. Assuming that the two members of the

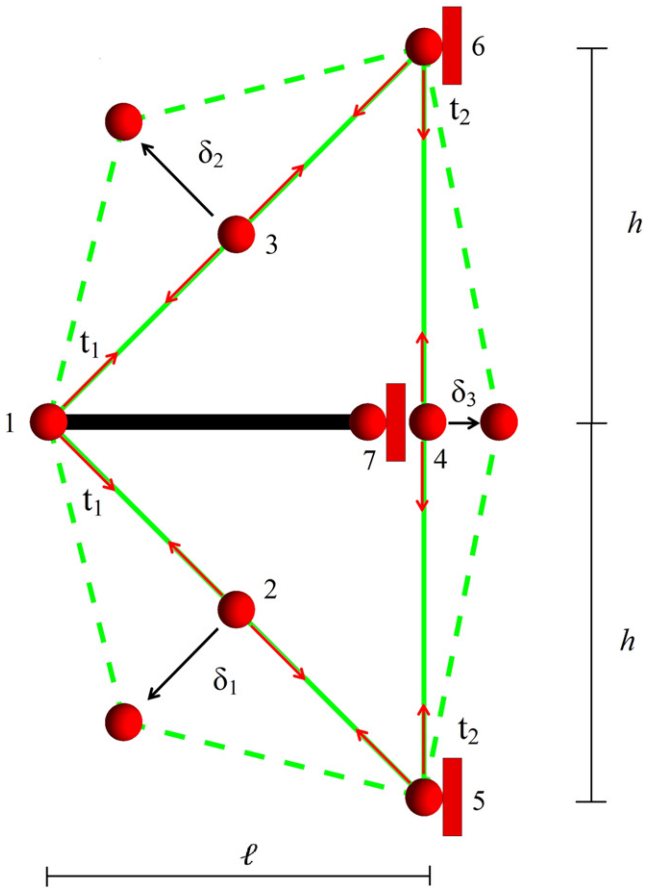

Figure 5. Elementary Venetian blind lattice in 2D.

lattice in figure 3 show equal axial stiffness k, length ℓ and rest-length $\bar{\ell}$, we obtain

$$\boldsymbol{K}_M = \begin{bmatrix} 2k & 0 \\ 0 & 0 \end{bmatrix}, \quad \boldsymbol{K}_G = \begin{bmatrix} 0 & 0 \\ 0 & \dfrac{2k\left(\ell - \bar{\ell}\right)}{\ell} \end{bmatrix}, \tag{22}$$

$$\boldsymbol{K}_T = \boldsymbol{K}_M + \boldsymbol{K}_G = \begin{bmatrix} 2k & 0 \\ 0 & \dfrac{2k\left(\ell - \bar{\ell}\right)}{\ell} \end{bmatrix}. \tag{23}$$

An arbitrary mechanism of the lattice under examination is therefore of the following kind: $\boldsymbol{u_M} = [0, \delta]^{\mathsf{T}}$, for arbitrary δ, and it obeys

$$\boldsymbol{K}_G \boldsymbol{u}_M \cdot \boldsymbol{u}_M = \frac{2k\ \delta^2\left(\ell - \bar{\ell}\right)}{\ell} > 0, \ \text{for}\ \ell > \bar{\ell}. \tag{24}$$

Condition (**23**) implies that the lattice in figure 3 exhibits positive geometric stiffness when the bars 1-2 and 1-3 are under nonzero pre-tension forces $t = k\ (\ell - \bar{\ell})$. In addition, it is possible to verify that it results in

$$\boldsymbol{K}_G \boldsymbol{u}_N \cdot \boldsymbol{u}_N = 0 \tag{25}$$

for any $\boldsymbol{u_N} = [\eta, 0]^{\mathsf{T}}$ that is not a mechanism. In other words, initial tensions in the bars 1-2 and 1-3 stabilize the lattice against vertical deflections δ of the central node 1 (lattice mechanisms), and induce zero geometric stiffness against virtual displacements that are not mechanisms (i.e., the lattice under consideration, which is trivially both kinematically and statically indeterminate of degree one, is superstable). The use of a superstable lattice for the actuation of a shading façade is illustrated in section 4.

We end the present section by noting that the presented results on the morphing and stability properties of tensegrity lattices, which are known in the literature, are aimed at demonstrating that such systems are well suited to the design of stable structures that can be actuated with limited storage of internal energy. The following sections illustrate practical uses of such features in designing innovative structures for kinetic facades of smart buildings.

3. 'Mashrabiya' sun screens with tensegrity architecture

The morphing abilities of the elementary lattice structure illustrated in figure 1 can be exploited to design a tensegrity solution for the actuated façade panels of the Al Bahar Towers in Abu Dhabi. Designed recently by Aedas Architects, using a different technology, such panels are intended to mimic the shading lattice-work 'mashrabiya' [18].

Let us assume that the x_3-axis of the elementary lattice in figure 1 is perpendicular to the building façade to be shaded, and that such a façade is placed at the node $x_3 = -2.00$ m. By inserting shading panels in correspondence with the triangular facets 1-4-3 and 2-4-3 of the elementary lattice, and replicating such a structure over space as shown in figure 4, we can form mashrabiya-like shading screens that can be opened and closed by actuating a single string for each elementary module.

The shading mechanism played by the generic 'eye' of such screens is graphically illustrated in figures 4(a)–(b). It assumes that the actuated strings are unstretched in correspondence with the open configuration of the eye, and subject to an axial strain $\bar{\varepsilon} = 6.25\%$ in correspondence with the fully-closed configuration. Such a mechanism has been numerically studied by integrating equation (8) through an explicit fourth-order Runge–Kutta scheme with step size $\Delta\varepsilon = 0.01\%$. An animation of the mechanism in figure 4 is given in the supplementary material. The force vectors depicted in figure 4 are proportional to the amplitude of the elongations of the actuated strings.

4. Venetian blind tensegrity screens

Figure 5 shows a planar lattice that mimics a Venetian blind. It is composed of a rigid members (thick black lines), and a chain-string (thin green line), which is pin-jointed to the rigid member, and is externally constrained by two fixed hinges. The rigid member corresponds to a slat (e.g. equipped with a PV module [12]). We insert internal hinges at the mid-spans of the segments composing the chain-string to account for zero bending rigidity of such members, which are transversally unstable in absence of prestress (see figure 3). It is not difficult to prove that the lattice in figure 5 is kinematically indeterminate of degree three, and statically indeterminate of degree two. On using the notation shown in figure 5, we characterize the mechanisms of such a structure through three displacement parameters δ_1, δ_2, and δ_3, and its state of prestress through the tensile forces t_1 and t_2, which respectively run along the external and internal branches of the chain-string (figure 5).

Let us order the free components of an arbitrary virtual displacement of the lattice of figure 5 into the following vector with eight entries $=[u_{1_1}, u_{1_2} \ldots, u_{4_1}, u_{4_2}]^{\mathsf{T}}$, with u_{i_1} and u_{i_2} respectively denoting the horizontal and vertical displacement components of node i. Assuming that all the string segments show equal axial stiffness k, we obtain the material and geometric stiffness matrices of such a structure as follows

$$\boldsymbol{K}_M = \begin{bmatrix} \frac{2\ell^2 k}{s} & 0 & -\frac{\ell^2 k}{s} & \frac{h\ell k}{s} \\ 0 & \frac{2h^2 k}{s} & \frac{h\ell k}{s} & -\frac{h^2 k}{s} \\ -\frac{\ell^2 k}{s} & \frac{h\ell k}{s} & \frac{2\ell^2 k}{s} & -\frac{2h\ell k}{s} \\ \frac{h\ell k}{s} & -\frac{h^2 k}{s} & -\frac{2h\ell k}{s} & \frac{2h^2 k}{s} \\ -\frac{\ell^2 k}{s} & -\frac{h\ell k}{s} & 0 & 0 \\ -\frac{h\ell k}{s} & -\frac{h^2 k}{s} & 0 & 0 \\ 0 & 0 & 0 & 0 \\ 0 & 0 & 0 & 0 \end{bmatrix} \begin{bmatrix} -\frac{\ell^2 k}{s} & -\frac{h\ell k}{s} & 0 & 0 \\ -\frac{h\ell k}{s} & -\frac{h^2 k}{s} & 0 & 0 \\ 0 & 0 & 0 & 0 \\ 0 & 0 & 0 & 0 \\ \frac{2\ell^2 k}{s} & \frac{2h\ell k}{s} & 0 & 0 \\ \frac{2h\ell k}{s} & \frac{2h^2 k}{s} & 0 & 0 \\ 0 & 0 & 0 & 0 \\ 0 & 0 & 0 & 2k \end{bmatrix} \tag{26}$$

$$\boldsymbol{K}_G = \begin{bmatrix} \frac{4h^2 \mathrm{t}_1}{s^{3/2}} & 0 & -\frac{2h^2 \mathrm{t}_1}{s^{3/2}} & -\frac{2h\ell \mathrm{t}_1}{s^{3/2}} \\ 0 & \frac{4\ell^2 \mathrm{t}_1}{s^{3/2}} & -\frac{2h\ell \mathrm{t}_1}{s^{3/2}} & -\frac{2\ell^2 \mathrm{t}_1}{s^{3/2}} \\ -\frac{2h^2 \mathrm{t}_1}{s^{3/2}} & -\frac{2h\ell \mathrm{t}_1}{s^{3/2}} & \frac{4h^2 \mathrm{t}_1}{s^{3/2}} & \frac{4h\ell \mathrm{t}_1}{s^{3/2}} \\ -\frac{2h\ell \mathrm{t}_1}{s^{3/2}} & -\frac{2\ell^2 \mathrm{t}_1}{s^{3/2}} & \frac{4h\ell \mathrm{t}_1}{s^{3/2}} & \frac{4\ell^2 \mathrm{t}_1}{s^{3/2}} \\ -\frac{2h^2 \mathrm{t}_1}{s^{3/2}} & \frac{2h\ell \mathrm{t}_1}{s^{3/2}} & 0 & 0 \\ \frac{2h\ell \mathrm{t}_1}{s^{3/2}} & -\frac{2\ell^2 \mathrm{t}_1}{s^{3/2}} & 0 & 0 \\ 0 & 0 & 0 & 0 \\ 0 & 0 & 0 & 0 \end{bmatrix} \begin{bmatrix} -\frac{2h^2 \mathrm{t}_1}{s^{3/2}} & \frac{2h\ell \mathrm{t}_1}{s^{3/2}} & 0 & 0 \\ \frac{2h\ell \mathrm{t}_1}{s^{3/2}} & -\frac{2\ell^2 \mathrm{t}_1}{s^{3/2}} & 0 & 0 \\ 0 & 0 & 0 & 0 \\ 0 & 0 & 0 & 0 \\ \frac{4h^2 \mathrm{t}_1}{s^{3/2}} & -\frac{4h\ell \mathrm{t}_1}{s^{3/2}} & 0 & 0 \\ -\frac{4h\ell \mathrm{t}_1}{s^{3/2}} & \frac{4\ell^2 \mathrm{t}_1}{s^{3/2}} & 0 & 0 \\ 0 & 0 & \frac{2\mathrm{t}_2}{h} & 0 \\ 0 & 0 & 0 & 0 \end{bmatrix}, \tag{27}$$

where $s = \boldsymbol{h}^2 + \boldsymbol{\ell}^2$. An inspection of equations (26) and (27) reveals that the structure in figure 6 is superstable when nonzero tensions $\mathbf{t}_1$ and $\mathbf{t}_2$ are applied to the external and internal branches of the chain-string, Such forces are indeed able to 'stabilize' the mechanisms depicted in figure 5, in such a way that it results $\mathbf{K_G}\,\mathbf{u_M} \cdot \mathbf{u_M} > \mathbf{0}$ in correspondence with all such mechanisms ($\mathbf{M} = 1, 2, 3$). In particular, one can tailor the state of prestress of the structure (i.e., the values of $\mathbf{t}_1$ and $\mathbf{t}_2$ under zero external forces) to the expected values of the horizontal forces that the structure is expected to carry (e.g., to the maximum wind-pressure).

A first actuation strategy of the lattice under examination is obtained by applying elongation rates $\pm\dot{\tilde{e}}$ with opposite signs to the diagonal elements 1-2-5 and 1-3-6 of the chain-string, and setting to zero the elongation rates of all the remaining string segments. Such an elongation rate vector $\dot{\tilde{\boldsymbol{e}}}$ produces a nodal velocity vector $\dot{\boldsymbol{q}}$ associated with an infinitesimally small rotation of the slat 1-7. By integrating the vector $\dot{\boldsymbol{q}}$ over time, over the current configuration of the lattice, we obtain the motion $\boldsymbol{q} = \int_0^t \dot{\boldsymbol{q}}\, \mathrm{d}t$, which is associated with a finite rotation of the slat 1-7. The actuation mechanisms under examination can be enforced by letting the nodes 5 and 6 to work as fixed pulleys (or drums) driven by an external motor, in such a way that the length decrease (or increase) of segments 1-2-5 of the chain-string is balanced by a length increase (or decrease) of segments 6-3-1. In such a

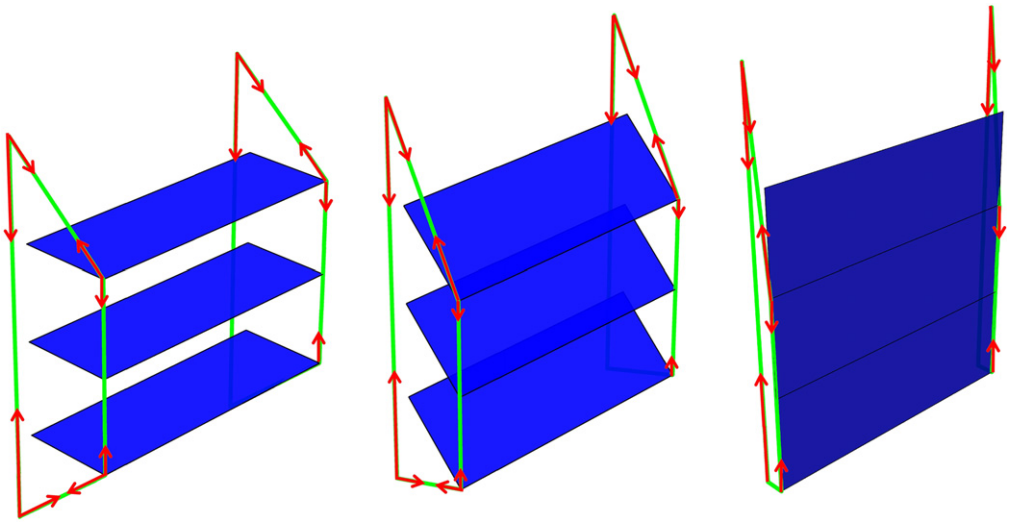

Figure 6. Sun-tracking actuation mechanism of a Venetian blind lattice with tensegrity architecture.

case, the chain-string is composed of a continuous cable with constant length. A three-dimensional version of the actuation strategy under examination is shown in figure 6, with reference to a three-slat Venetian blind system obtained by piling up three slat elements. Figure 6 illustrates that such an actuation mechanism leads to design wind-stable blinds with orientable slats, which can be controlled by a motor connected to a single pulley for each chain-string. It requires limited contact surfaces and friction effects (between the chain and the grooves of the pulleys). The force vectors depicted in figure 6 are proportional to the amplitude of the forces carried by the strings in correspondence with the examined configurations, assuming equal force densities in the top diagonal element of the external branch of the chain string, and in the internal branch of the chain string.

A slat-rail mechanism can be instead employed to produce the vertical deployment (or vertical collapse) of the blind, which may be required, e.g., to operate maintenance operations on the façade served by the structure. Such a mechanism is produced by releasing the pre-tension t applied to the chain string, applying vertical displacements to internal extremities of the slats along guiding rails, and applying a final rotation to the packed slats (figure 7). It is worth observing that such a mechanism is necessary only in occurrences of singular maintenance interventions.

5. Future perspectives

The use of tensegrity structures for the construction of renewable energy supplies requires attention, because of the special ability of such structures to convert the strain energy stored in cables into electrical energy [9], and their easy integration with solar and/or acoustical panels, which can be identified with rigid members of the structure. It is worth noting that the operation of the 'mashrabiya' shading screens presented in section 3 can be powered by the renewable energy derived from photovoltaic panels and/or microeolic power generators. Their aim is to markedly mitigate air conditioning consumption resulting from direct exposure to solar rays, reducing carbon dioxide emissions. The morphing screen analyzed in section 3 requires minimal storage of internal energy [25], and reduced operation costs (because of the lighter friction between parts and reduced mass) compared, for instance, to the piston-actuated technology adopted by Aedas Architects [18]. Similarly, the wind-stable Venetian blind screens analyzed in section 4 require light friction effects and reduced contact surface areas when operating in sun-tracking mode compared, e.g., to more conventional slat-rail mechanisms [15–17]. We base our claims on the economical convenience of the above structures, over more conventional renewable energy supplies, on qualitative but solid arguments, that are inspired by the lightweight nature, reduced friction effects between parts (concentrated at the nodes), and the morphing abilities of tensegrity systems.

Future extensions of the present study will deal with the design of bioinspired skins of energy-efficient buildings [30–32], which will combine morphing abilities with prestress-stability. Such structures will be able to orient solar panels toward the sun, to adjust the thickness of ventilated walls, and/or to form innovative microeolic power generators (figure 8). They will assemble tensegrity units of various shapes and materials. Each unit will be equipped with sensors and actuators in correspondence with selected elements, which will be connected by wires or wireless devices to a data transfer system. It will operate in two basic regimes: energy harvesting mode (EH mode), and control mode (CT mode). In the EH mode, the elongation of the cables will rotate an external generator, creating power to be used for the operation of the building. In the CT mode, an external motor will adjust the tension of the cables and/or the length or the orientation of the rigid elements, by controlling the actuators inserted into the unit (figure 8). The results of the present study will serve as seminal work for the design of the actuation mechanisms of such structures, and the analysis of their stability. We plan to fabricate reduced scale models of morphing and stable skins

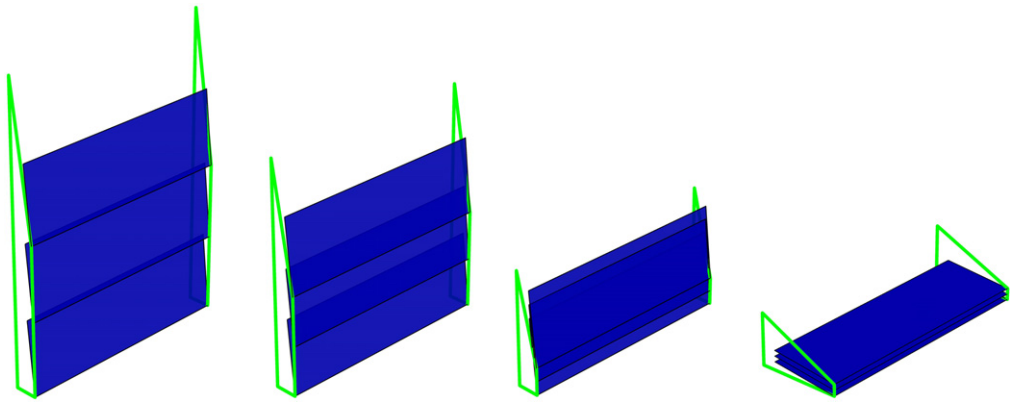

Figure 7. Vertical deployment mechanism of the Venetian blind lattice.

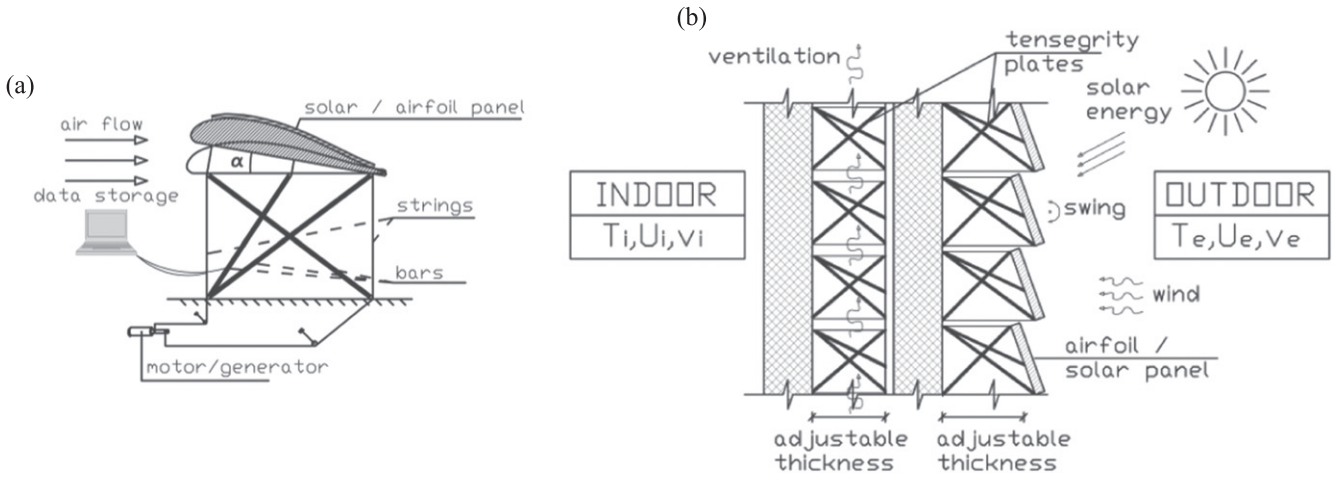

Figure 8. Morphing skins of energy efficient buildings based on tensegrity structures: (a) tensegrity unit; (b) responsive solar façade and ventilated wall.

of smart buildings via additive manufacturing. An experimental validation phase will investigate the mechanical response and the control of such models. It will lead to an evaluation of the scalability of the proposed solutions and the associated economic benefits.

Additional future research lines may regard the optimal design of polyhedral envelopes [9, 33] of energy-efficient buildings, to be carried out by combining parametric design approaches with energy-optimization techniques.

6. Concluding remarks

We have presented an application of morphing and super-stable lattices with tensegrity architecture to design adaptable shading screens for energy efficient buildings. We have designed 'origami' screens exhibiting morphing 'eyes', which are opened and closed by controlling the elongation in a limited number of cables. We have also designed a super-stable tensegrity structure that replicates a wind-stable Venetian blind. All the tensegrity structures analyzed in the present work offer portable applications for small spans, and can be assembled for prefabricated component parts in the case of large spans. Future directions of the study presented in this work are drawn in section 5.

Acknowledgments

Support for this work was received from the Italian Ministry of Foreign Affairs, Grant no. PGR00173/2015, Italy-USA Scientific and Technological Cooperation 2015.

References

[1] Lombard L P, Ortiz J and Pout C 2010 A review on buildings energy consumption information *Energy Build.* **40** 394–8
[2] European Commission 2014 *HORIZON 2020 Work Programme 2014–2015, Part 5.ii* (European Commission) p 98 (https://ec.europa.eu/research/participants/data/ref/h2020/wp/2014_2015/main/h2020-wp1415-leit-nmp_en.pdf)
[3] Balduzzi F, Bianchini A and Ferrari L 2012 Microeolic turbines in the built environment: influence of the installation site on the potential energy yield *Renew. Energy* **45** 163–74

[4] Kuhn T E, Herkel S and Henning H-M 2010 Active solar facades (PV and solar thermal) *Palenc 2010* (http://publica.fraunhofer.de/documentsN-161087.html)
[5] Quesada G, Rousse D, Dutil Y, Badache M and Hallé S 2012 A comprehensive review of solar facades. Opaque solar facades *Renew. Sust. Energ. Rev.* **16** 2820–32
[6] Quesada G, Rousse D, Dutil Y, Badache M and Hallé S 2012 A comprehensive review of solar facades transparent and translucent solar facades *Renew. Sust. Energ. Rev.* **16** 2643–51
[7] Schittich C (ed) 2003 *In Detail: Solar Architecture* (Basel: Birkhäuser)
[8] Skelton R E 2002 Structural systems: a marriage of structural engineering and system science *J. Struct. Contr.* **9** 113–33
[9] Skelton R E and de Oliveira M C 2010 *Tensegrity System* (Berlin: Springer)
[10] Hien W N, Liping W, Chandra A N, Pandey A R and Xiaolin W 2005 Effects of double glazed facade on energy consumption, thermal comfort and condensation for a typical office building in Singapore *Energy Build.* **37** 563–72
[11] Gratia E and De Herde A 2007 The most efficient position of shading devices in a double skin facade *Energy Build.* **39** 364–73
[12] Kang S, Hwang T and Kim J T 2012 Theoretical analysis of the blinds integrated photovoltaic modules *Energy Build.* **46** 86–91
[13] Ji Y, Cook M J, Hanby V, Infield D G, Loveday D L and Mei L 2008 CFD modelling of naturally ventilated double-skin facades with Venetian blinds *J. Build. Perform. Simul.* **1** 185–96
[14] Nemati O 2009 Analysis of a mechanically ventilated multiple-skin façade with between-the-panes venetian blinds *MSc Thesis* University of Waterloo, Ontario, Canada
[15] Buser F 2011 *Germany Patent Application* EP20,100,405,158 (https://google.it/patents/EP2312112A1?cl=en)
[16] Liang S G, Li D, Zhang G B and Wen X 2013 *China Patent Application* CN201,310,049,530 (https://google.it/patents/CN103114798A?cl=en)
[17] Warema, wind-stable Venetian blinds, (http://shadefactor.com.au/external-venetian-blinds/external-venetian-blinds/item/20-wind-stable-venetian-blinds)
[18] Al Bahar Towers Responsive Facade/Aedas, (http://archdaily.com/270592/al-bahar-towers-responsive-facade-aedas/)
[19] Skelton R E, Fraternali F, Carpentieri G and Micheletti A 2014 Minimum mass design of tensegrity bridges with parametric architecture and multiscale complexity *Mech. Res. Commun.* **58** 124–32
[20] Fraternali F, Carpentieri G and Amendola A 2014 On the mechanical modeling of the extreme softening/stiffening response of axially loaded tensegrity prisms *J. Mech. Phys. Solids* **74** 136–57
[21] Fraternali F, Senatore L and Daraio C 2012 Solitary waves on tensegrity lattices *J. Mech. Phys. Solids* **60** 1137–44
[22] Fraternali F, Carpentieri G, Amendola A, Skelton R E and Nesterenko V F 2014 Multiscale tunability of solitary wave dynamics in tensegrity metamaterials *Appl. Phys. Lett.* **105** 201903
[23] Tilbert A G and Pellegrino S 2012 Review of form-finding methods for tensegrity structures *Int. J. Space Struct.* **18** 209–23
[24] Hutchinson R G and Fleck N A 2012 The structural performance of the periodic truss *J. Mech. Phys. Solids* **54** 756–82
[25] Fleck N A, Deshpande V S and Ashby M F 2010 Micro-architectured materials: past, present and future *Proc. R. Soc.* A **466** 2495–516
[26] Guest S D 2006 The stiffness of prestressed frameworks: a unifying approach *Int. J. Solids Struct.* **43** 842–56
[27] Schenk M, Guest S D and Herder J L 2007 Zero stiffness tensegrity structures *Int. J. Solids Struct.* **44** 6569–83
[28] Micheletti A 2013 Bistable regimes in an elastic tensegrity system *Proc. R. Soc.* A **27** 20130052
[29] Favata A, Micheletti A and Podio-Guidugli P 2014 A nonlinear theory of prestressed elastic stick-and-strings structures *Int. J. Eng. Sci.* **80** 4–20
[30] Fraternali F, Lorentz C D and Marcelli G 2012 On the estimation of the curvatures and bending rigidity of membrane networks via a local maximum-entropy approach *J. Comput. Phys.* **231** 528–40
[31] Fraternali F and Marcelli G 2012 A multiscale approach to the elastic moduli of biomembrane networks *Biomech. Model. Mech.* **11** 1097–108
[32] Schmidt B and Fraternali F 2012 Universal formulae for the limiting elastic energy of membrane networks *J. Mech. Phys. Solids* **60** 172–80
[33] Fraternali F, Farina I and Carpentieri G 2014 A discrete-to-continuum approach to the curvatures of membrane networks and parametric surfaces *Mech. Res. Commun.* **56** 18–25